Full-Metal Omnidirectional Filtenna Array Using 3-D Metal Printing Technology

Shu-Qing Zhang, *Student Member, IEEE*, Sai-Wai Wong, *Senior Member, IEEE*, Zhonghe Zhang, *Graduate Student Member, IEEE*, and Yejun He, *Senior Member, IEEE*

***Abstract*— This article proposes a full-metal omnidirectional series-fed filtenna array. The antenna is primarily composed of an outer metal shell, a built-in metal post and three pairs of open-circuit branches. To achieve horizontal omnidirectional radiation, a circular groove is dug on the outer metal shell. Additionally, the built-in metal post is connected to the coaxial feed and shorted at the end with the outer shell. The antenna's filtering principle can be interpreted as a second-order bandpass filter without any transmission zeros. To enhance out-of-band suppression, three pairs of open stubs have been introduced. And then, three radiation nulls are incorporated to improve frequency selectivity and out-of-band suppression without increasing additional circuit size. Finally, a 3-D-printed series-fed filtenna has been fabricated and measured. The −10-dB $|S_{11}|$ impedance fractional bandwidth is 3% (ranged from 2.79 to 2.875 GHz), the antenna peak gain is 6.6 dBi, and the three radiation nulls are located at 2.55, 2.69, and 3.09 GHz, respectively. The measured out-of-band suppression is 28 dB.**

***Index Terms*— Filtenna, full-metal, high-selectivity, omnidirectional, series-fed antenna.**

I. Introduction

In A wireless communication system, the antenna plays a crucial role as it receives all external radio frequency (RF) signals before they undergo further signal processing. With the increasing demand for large-area signal coverage in modern communication, antennas are now faced with more challenging requirements as they receive not only signals but also more interference. Thus, good out-of-band suppression is particularly important due to the extremely dense of spectrum resources in commercial wireless communication. To solve this problem, a filtering function should be added to this kind of antenna to become a filtenna. Filters play an essential role in eliminating unwanted near-band signals or interference noise. However, the traditional method of cascading filters with antennas will inevitably increase the circuit size. As high integration is a key trend in the development of RF circuits, there is a growing need to reduce the space occupied by RF devices. To address this, antennas with integrated filtering functions have emerged, combining the functionalities of both the filter and the antenna [1], [2]. This integration allows for more compact RF designs while maintaining the necessary filtering capabilities.

After decades of development, various types of filtennas have been reported in the literature, employing different technologies. These include patch filtennas [1], [2], [3], [4], [5], filtering dielectric resonator antennas (FDRAs) [6], [7], [8], [9], [10], [11], [12], [13], substrate integrated waveguide/cavity filtennas [14], [15], [16], [17], [18], [19], dipole filtennas [20], [21], and others. According to the design method of filtennas, they can be broadly classified into two categories: filter-based design method and antenna-based design method. In the filter-based design method, the antenna is considered as the last resonator and output port of the filter. In [23], a microstrip antenna is connected to the end of the bandpass filter. This filtenna not only acts as a radiator but also serves as the second order filter, which achieves 13 dB out-of-band suppression. Su et al. [21] proposed that a series-fed antenna is designed based on the principle of a second-order bandpass filter to achieve better harmonic suppression performance. Lin et al. [24] proposed that a technique is described where two sets of different slots are regularly etched on the cavity according to the magnetic field distribution of the high-order mode. This approach enables the realization of a dual-frequency dual-polarization filtenna.

From the perspective of antenna design, there are three main methods that can be employed. The first method involves incorporating a band-stop parasitic structure into the antenna. In [25], the parasitic structure is loaded on both sides of the microstrip feed line to provide good out-of-band suppression for the upper stopband, the out-of-band suppression larger than 25 dB; the second design method involves integrating short-circuit metal pillars, gaps, or parasitic elements into the antenna design, which can be utilized to modify the electric field or magnetic field, or alter the surface current distribution. This is a widely used design technique in filtenna design. In [26], a low-frequency null is generated through a diagonal slot, and a high-frequency null is generated through an E-shaped slot. In [9], by adding three sets of different metal pillars in the dielectric resonator, the original electric field distribution is changed while the mode is transferred, two radiation nulls are generated, and the out-of-band suppression exceeds 14 dB. Similarly, [27], [28] demonstrated

Manuscript received 27 September 2023; revised 24 March 2024; accepted 2 April 2024. Date of publication 12 April 2024; date of current version 7 May 2024. This work was supported by the National Natural Science Foundation of China under Grant 62171289. *(Corresponding author: Sai-Wai Wong.)*

The authors are with the State Key Laboratory of Radio Frequency Heterogeneous Integration, College of Electronics and Information Engineering, Shenzhen University, Shenzhen 518060, China (e-mail: wongsaiwai@ieee.org).

Color versions of one or more figures in this article are available at https://doi.org/10.1109/TAP.2024.3385914.

Digital Object Identifier 10.1109/TAP.2024.3385914

that a low-frequency radiation null could be achieved by incorporating short circuit metal posts, while [29] showed that introducing four parasitic patches around the main patch not only induced a resonant mode but also introduced a radiation null. Finally, a multielement structure and special feeding design methods can also be used, such as the method of transverse coupling can produce several radiation nulls [30]. In [31], three independently designed patch antennas are used. When all three antennas are excited simultaneously, the patches located on both sides of the main radiating patch can each cancel out with the main radiating patch to create two radiation nulls; likewise, in [32], the antenna is fed through multiple paths, causing a radiation cancellation between the patches, resulting in a high-frequency radiation null. While there have been numerous studies on filtennas and omnidirectional antennas individually, there has been relatively less research conducted on the combination of filters and omnidirectional antennas [33], [34], or on full-metal antennas [35], [36], [37].

Due to the large area coverage of omnidirectional antenna, filtering function is particularly important than other kind of antenna. In this work, a full-metal omnidirectional series-fed filtenna based on 3-D metal printing technology is proposed. The proposed filtenna design features a metal post series-fed antenna structure that radiates electromagnetic (EM) energy through four circular slots. In order to achieve better frequency selectivity without increasing the size of the antenna, some metal open branches are introduced. The filtenna is fabricated using advanced manufacturing techniques and subjected to rigorous testing. The measured results demonstrate excellent agreement with the simulation, validating the effectiveness of the proposed design. This article is organized as follows. Section II discusses the antenna principle, Section III focuses on antenna design, Section IV covers antenna fabrication and measurement, at the same time, the performance of the proposed filtenna is compared with some previous antennas in Table I. Section V provides a conclusion, followed by an appendix that includes some fundamental theories related to the proposed antenna and the impact of certain parameters on performance.

II. Antenna Principle

Fig. 1(a) depicts a simple series-fed antenna array, which serves as a basic electrical model for the filtenna proposed in this article. It is important to note that this model does not take into account the actual physical support provided by the outer metal shell, nor does it consider the radiation pattern performance. These aspects will be further refined and improved in Section III of the article. Section III will provide more detailed explanations and enhancements regarding these aspects of the filtenna design.

Next, the equivalent circuit is used to qualitatively analyze the omnidirectional series-feed antenna array. Fig. 1(c) and (b) are the equivalent circuit diagrams of N elements and two elements, respectively. The series-fed antenna can be modeled as a second-order filter circuit, as described in [20]. As a result, it possesses inherent filtering capabilities and can exhibit certain filtering performance. The loaded annular slot antenna can be equivalently represented as a section of

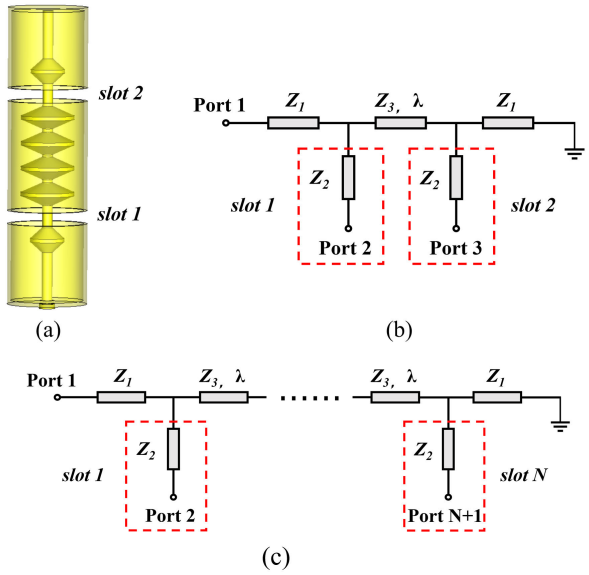

Fig. 1. (a) Preliminary model of two-elements series-fed antenna array. (b) Preliminary equivalent circuit model of two-element antenna array. (c) Preliminary equivalent circuit model of N-element antenna array.

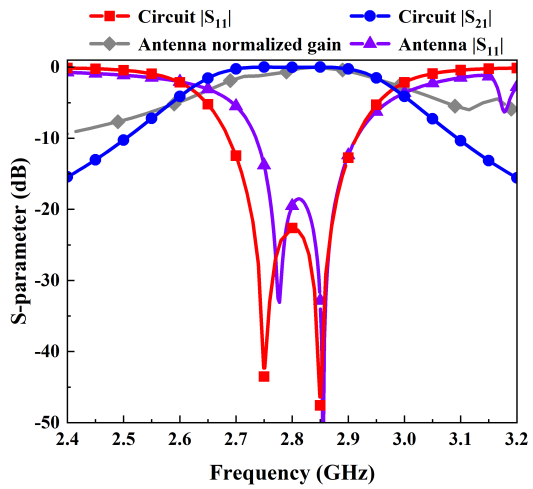

Fig. 2. Circuit simulation and CST model simulation results.

transmission line Z_2, along with either port 2 or port 3. The Z_2 represents the resonance characteristics of the slot antenna, while the ports represent the energy radiated by the slot antenna. Assuming that all the radiated energy can be collected to ports 2 and 3, Z_1 and Z_3 are equivalent to series-fed, and this circuit diagram can also be expanded into a series-fed antenna array with multiple array elements. Fig. 1 illustrates a three-port network, where the total energy radiated by the antenna is equivalent to the sum of the energy collected at port 2 and port 3. Since Z_3 has a length corresponding to one wavelength or 360° electrical degrees, we can combine ports 2 and 3 to create a virtual port 2, then $|S_{21}|$ of the network can be calculated according to the law of energy conservation as follows, $|S_{21}| = \sqrt{1 - |S_{11}|^2}$. Fig. 2 compares the simulation results of the circuit and antenna shown in Fig. 1(a). It is evident that the $|S_{11}|$ of the two models are reasonable consistent, but the gain curve of the circuit model simulation is slightly different from the $|S_{21}|$ of the circuit simulation, this is reasonable because circuit simulation is an

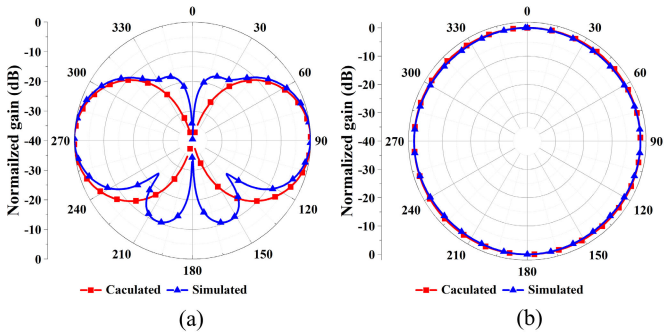

Fig. 3. Computational and CST model simulation radiation patterns. (a) E-plane. (b) H-plane.

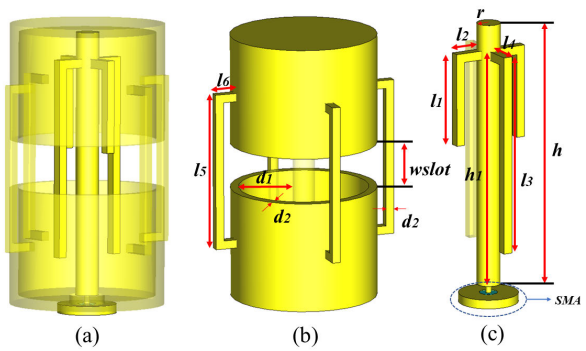

Fig. 4. Structural diagram of case-A filtenna. (a) Three-dimensional view. (b) External structural diagram. (c) Internal structural diagram.

ideal equivalent model, while full-wave simulation includes the influence of various parasitic effects on the overall performance of the antenna. This initial two-element two antenna arrays will be introduced in Section III.

According to the equivalence circuit model between the annular slot antenna and the short electric dipole discussed above, the radiation pattern E-plane and H-plane of the series-fed antenna can be approximately calculated according to (1) and (2), and the radiation pattern of model simulated as shown in Fig. 3(a) and (b), respectively,

$$E(\theta,\phi) = j\frac{60I}{r}\frac{cos\left(\frac{\pi}{2}cos\theta\right)}{sin\theta}2cos\left(\frac{kd}{2}cos\theta\right)e^{-jkr} \quad (1)$$

$$f(\theta,\phi) = \frac{|E(\theta,\phi)|}{E_{MAX}}. \quad (2)$$

From the circuit model simulation and full-wave simulation results, it can be seen that the antenna has omnidirectional radiation performance and has certain filtering performance. However, there are no transmission zeros which means poor frequency selectivity. Next, the filtering performance will be further improved, and the antenna array will be composed of a ring-shaped filtenna.

III. Antenna Design

A. Case-A

Fig. 4(a) displays the overall structure of case-A filtenna, which consists of three main components: the outer metal shell, the inner metal post, and the coaxial feed located at the bottom. Furthermore, Fig. 4(b) illustrates that a slot antenna is formed along the outer metal shell of this filtenna to achieve omnidirectional radiation. To ensure sufficient physical support for the metal shell, four half-wavelength shorting branches are incorporated across the slot. These branches serve the dual purpose of providing physical support and grounding effects at both the lower and upper metal shell. Fig. 4(c) visually depicts the internal structure of the proposed filtenna, showcasing the arrangement of open stubs within the antenna design. The filtenna design includes two pairs of quarter-wavelength open stubs, each corresponding to their respective radiation null frequencies located at the lower and upper stopband. Furthermore, the inner metal post is short-circuited at the top with the outer metal shell, which provides a third radiation null at the lower stopband. These design features contribute

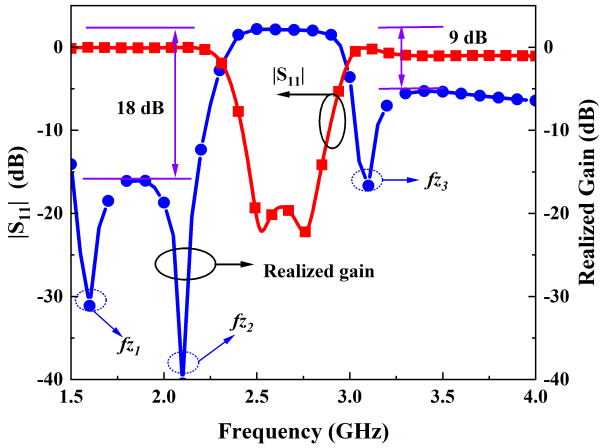

Fig. 5. Simulation S parameter and gain curve of case A.

to improved filtering performance and enhanced radiation characteristics of the filtenna

$$f_{z1} = \frac{c}{4(l_1 + l_2)} \quad (3)$$

$$f_{z2} = \frac{c}{2h} \quad (4)$$

$$f_{z3} = \frac{c}{4(l_3 + l_4)}. \quad (5)$$

To mitigate the effects of structural asymmetry on the radiation pattern, the same length of open stubs is symmetrically placed around the inner metal post as the center of symmetry. This approach helps ensure a more balanced radiation pattern and reduces potential deviations caused by structural asymmetry.

The frequency of radiation nulls can be estimated using (3)–(5). In these equations, $(l_1 + l_2)$ represents the length of the short branch, h corresponds to the height of the antenna, and $(l_3 + l_4)$ denotes the length of the long branch. By substituting appropriate values into these equations, the frequency of radiation nulls can be approximated. Fig. 5 shows the S-parameter and gain curve of case-A. It can be seen that the center frequency of passband of the filtenna is 2.65 GHz, the impedance bandwidth of $|S_{11}|$ less than -10 dB is 18.16% (2.43–2.916 GHz), the lower stopband has two radiation nulls at 1.59 and 2.1 GHz, and the low frequency out-of-band suppression achieves 19 dB, the upper stopband has a radiation null at 3.09 GHz, and the out-of-band suppression

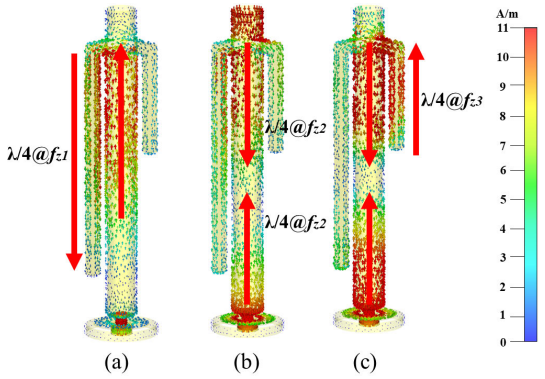

Fig. 6. Surface current distribution of case A at frequency of radiation nulls. (a) 1.59 GHz. (b) 2.1 GHz. (c) 3.09 GHz.

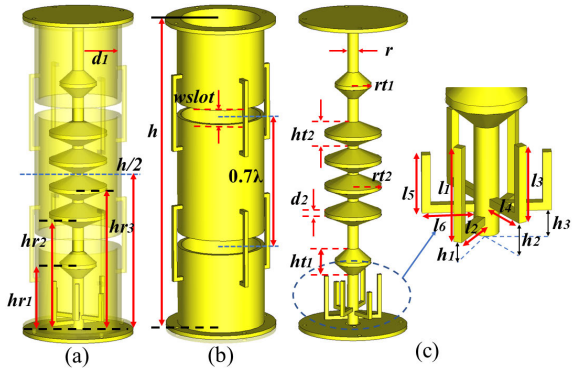

Fig. 7. Structural diagram of case-B filtenna. (a) Three-dimensional view. (b) External structural diagram. (c) Internal structural diagram.

achieves 9 dB, the slight discrepancy between the calculated result from (3) to (5) and the optimized result is likely due to the consideration of parasitic effects in the overall antenna design. Fig. 6(a) and (b) shows the current distribution at two low-frequency radiation nulls, and Fig. 6(c) shows the current distribution at high-frequency radiation nulls. f_{z1} is generated by a pair of long stubs, and f_{z3} is generated by a pair of short stubs. The EM energy at f_{z1} and f_{z3} is mainly concentrated on the open stub without radiating into the free space, while f_{z2} is generated due to the half-wavelength short-circuit of the inner metal post.

The impact of certain important parameters on the radiation nulls are shown in the appendix. Table II shows the size of the optimal simulation results of case-A filtenna.

B. Case-B

It can be seen from the filtenna gain curve in Fig. 5 that the in-band gain of the antenna is 2 dBi, and the high-frequency suppression level is 9 dB, in order to further increase the gain and improve the filtering performance, the case-B filtenna shown in Fig. 7 is proposed. The antenna features two slots on the metal shell specifically positioned for achieving omnidirectional radiation. These slots are symmetrically located about the plane at a height of $h/2$, ensuring balanced radiation patterns in all directions. To optimize the radiation performance, it is essential to position the slots at the height where the current density is the strongest. This ensures that the maximum

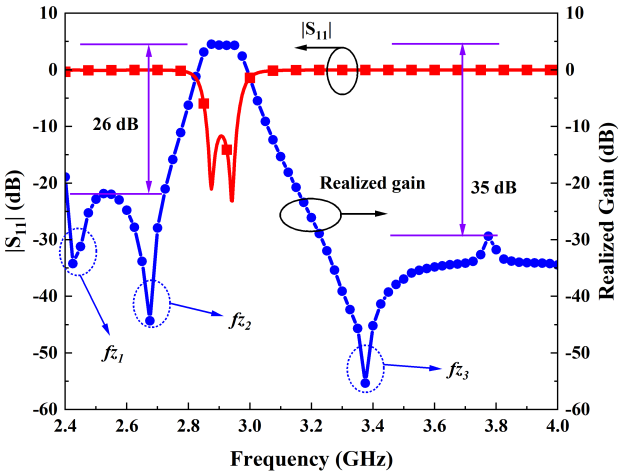

Fig. 8. Simulation S parameter and gain curve of case-B.

EM energy is radiated from the antenna. Additionally, in order to enhance the gain, it is important for the EM energy radiated by the two slots to superimpose on each other. To achieve this, the current densities of the metal pillars at the height of the two slots should be in phase. By aligning the phases of the current densities, the constructive interference between the radiated waves from the slots can be maximized, resulting in increased antenna gain.

For improving the filtering performance of the case-A, the open branches were increased to three groups as shown in Fig. 7(c). In the electrical circuit model of the case-B filtenna discussed in Fig. 1, it is observed that the electrical length between two radiation elements, port 2 and port 3, is only one wavelength apart. However, this configuration does not meet the requirement for achieving a good radiation pattern in the antenna array. To ensure the in-phase property between two radiation elements and achieve a good radiation pattern, it is indeed crucial to maintain the electrical length of the Z_3 element at one wavelength. Indeed, if it is necessary to reduce the physical length of the Z_3 element while maintaining the desired electrical length and in-phase property between radiation elements, techniques such as meandering or folding can be implemented. By implementing these techniques, it is possible to achieve a shorter physical length without compromising the in-phase property between the radiation elements. For reducing the physical length of Z_3 of the filtenna, some protruding slow wave structures were added to the built-in inner metal post, and the distance between the two slot antennas was reduced to about half a wavelength to satisfy the condition of superimpose of two slot elements, the six slow wave structures are symmetrical about the plane with height $h/2$ as shown in Fig. 7(a).

As shown in Fig. 8, it is the simulated S-parameter and gain curve of case-B filtenna. The passband center frequency of the filtenna is 2.9 GHz, and the −10-dB impedance bandwidth of $|S_{11}|$ is 3.4% ranged from 2.863 to 2.964 GHz. Fig. 9 is a fullwave simulation of the current distribution at the center frequency point with electromagnetic bandgap (EBG) [35], [36] structure between two radiation slots. Indeed, the highest current density is observed at the positions of the two slots

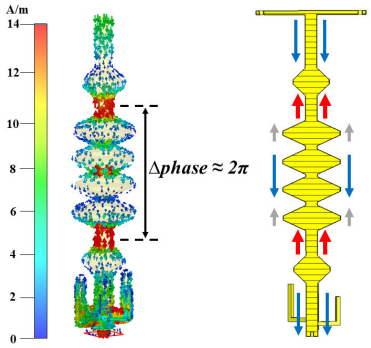

Fig. 9. In-band current diagram of case-B.

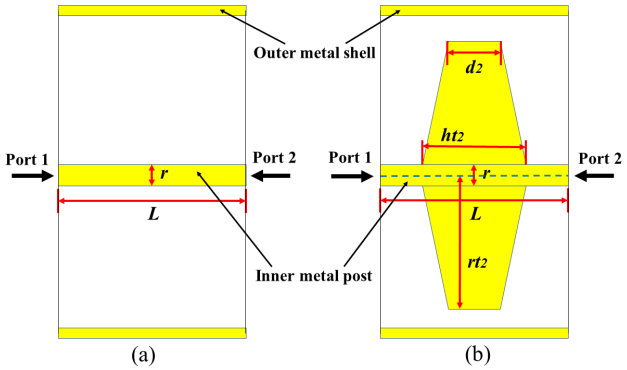

Fig. 10. Structural diagram of a single EBG structural. (a) Without EBG. (b) With EBG.

where radiation occurs. These high-density regions are indicated by the red arrows. Additionally, the phase between the two radiation slots is specifically designed to have an electrical length of 360°, ensuring they are in phase with each other. This phase alignment enables constructive interference and enhances the overall radiation performance of the antenna. The EBG structure serves an additional purpose of enabling slow wave propagation, which helps reduce the overall physical length of the two radiation elements. Without the EBG structure, the physical length of the two radiation slots would need to be one wavelength to achieve the desired in-phase condition. However, this would result in an undesired radiation pattern. Adding a EBG structure can reduce the physical length between the slots to half a wavelength, which meets the optimal spacing for forming an array with good radiation pattern. Meanwhile, the electrical length of the two slots is one wavelength in phase due to the slow wave property of the EBG structure.

Fig. 10 is a schematic of a single EBG unit. In the following analysis, we will examine the effect of slow wave behavior. In Fig. 10(a), a metal post is integrated into the filtenna without a slow wave structure. To investigate the transmission characteristics of this configuration, we extract the guided-wave propagation constants ($\gamma = \alpha + j\beta$) from its Z-matrix [38], [39], [40]. According to the Z-matrix, $ABCD$ matrix can be obtained, then the propagation constant γ can be calculated by the following equation:

$$cosh(\gamma L) = \frac{A + D}{2} \tag{6}$$

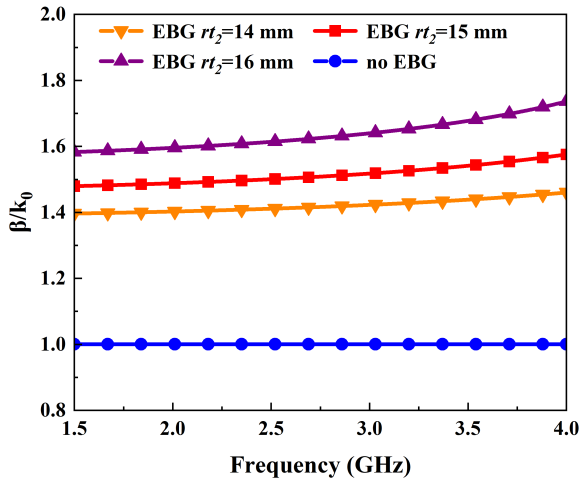

Fig. 11. Phase constant comparison with and without EBG structure.

where L is the physical length of an EBG structure. The extracted phase constant β/k_0 is shown in Fig. 11, where k_0 is the phase constant in free space. It can be observed that the phase constant of the EBG structure is approximately 0.5 times greater than that of the uniform unit without EBG structure. This indicates that, in the absence of EBG structure, the electrical length required is one wavelength, and the physical length is also one wavelength. By incorporating the EBG structure, it becomes possible to maintain a phase difference of 2π, while reducing the physical length of the radiation elements to half a wavelength. In this way, the goal of smaller array element spacing can be achieved with in-phase radiation, which is consistent with the original intention of designing the EBG structure. Fig. 11 also compares the β/k_0 corresponding to different rt_2. It can be seen that when rt_2 gradually increases, β/k_0 also increases, the phase change after the current flows through the EBG is greater; this implies a stronger slow wave effect.

Fig. 11 illustrates the performance of a single EBG. Next, we analyze the EBG structure used in case-B. As illustrated in Fig. 12, the red line represents the phase shift after current passes through the EBG structure of case-B, approximately 11°. The green line depicts the phase shift when the line is of the same length but without an EBG structure, with a phase difference of the current at the center frequency of the two lines being about 250°. This indicates that the currents between the two annular slots in case-B are in phase. The reason the phase difference here is not a perfect 180° shows that the distance between the two annular slots is not a perfect half wavelength, but about 0.7λ after the antenna gain optimization.

From the gain curve, it is evident that the lower stopband exhibits two radiation nulls, resulting in an out-of-band rejection of 26 dB. On the other hand, the upper stopband displays a radiation null, leading to an impressive out-of-band rejection of 35 dB. Compared with case-A filtenna, the high-frequency filtering performance has been greatly improved. The realized gain is 4.5 dBi in the passband. The three radiation nulls of case-B filtenna are all generated by three open stubs. According to formula (4), the radiation null generated by

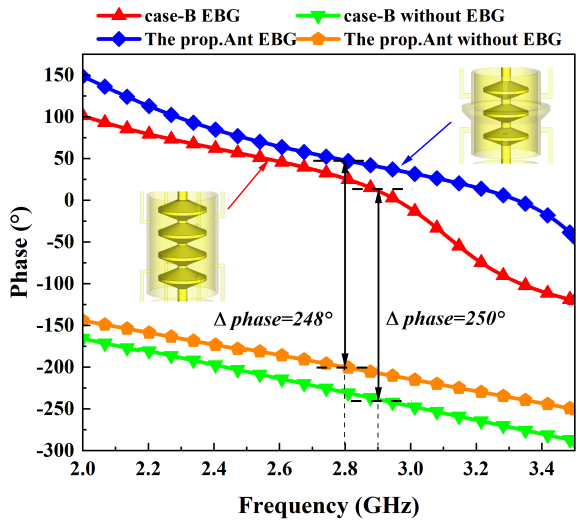

Fig. 12. Phase change comparison between two annular slots with and without EBG structure (case-B EBG: case-B filtenna with EBG, case-B without EBG: case-B filtenna without EBG, The prop.Ant EBG: The proposed filtenna with EBG, The prop.Ant without EBG: The proposed filtenna without EBG).

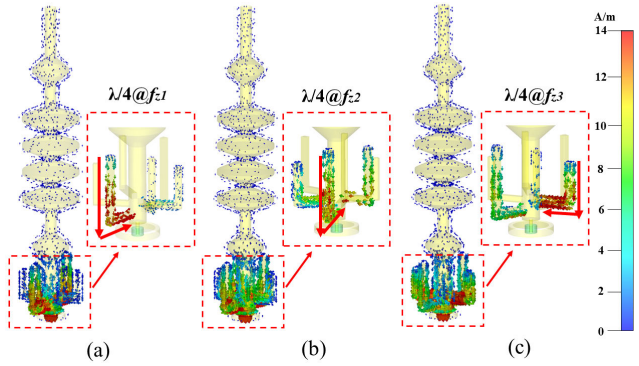

Fig. 13. Current distribution at radiation nulls of case B. (a) fz_1. (b) fz_2. (c) fz_3.

the half-wavelength short-circuit relationship has a frequency near 0.92 GHz and is far away from the central frequency band, so it does not have much significance effect for the filtering performance. This is why case-B filtenna only uses open stubs to generate radiation nulls near passband. Fig. 13 shows the current diagram at the three radiation nulls. Similar to the case-A, at this specific frequency point, the EM energy is primarily concentrated on the three pairs of open stubs. Instead of radiating into free space, the EM energy is confined within these stubs. The effects of certain key parameters on the radiation nulls are presented in the appendix. Table III shows the size of the optimal simulation results of case-B.

C. Proposed Antenna

Fig. 14 illustrates the block diagram of the proposed antenna design. To enhance the omnidirectional radiation gain, a four annular slots filtenna configuration is introduced. The positions of the four slots are symmetrically arranged about the plane at a height of $h/2$. Additionally, three sets of open-circuit branches are incorporated into the built-in metal post connected to the feeding coaxial cable transmission line.

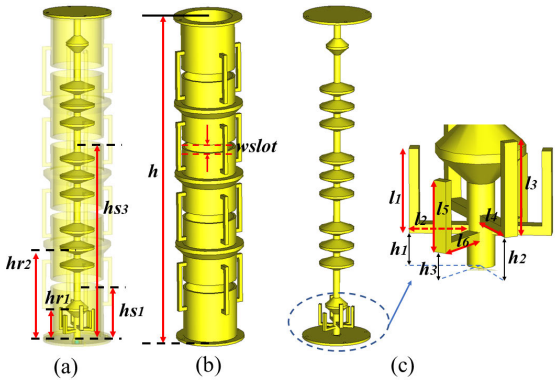

Fig. 14. Structural diagram of the proposed filtenna. (a) Three-dimensional view. (b) External structural diagram. (c) Internal structural diagram.

To facilitate the fabrication process, three ring-shaped structures resembling circular frustums are added to the metal shell. These structural additions help meet the requirements of the manufacturing process while ensuring the desired performance of the antenna. The primary difference between the proposed filtenna and the EBG structure in case-B is the number of EBG structures used to achieve better impedance matching. The proposed filtenna utilizes three EBG structures, while case-B employs four EBG structures. Based on the phase change between the two annular slots depicted in Fig. 12, it can be observed that at the center frequency, there is an approximate phase difference of 45°. Despite this phase difference, the performance remains close to an electrical length of 0°, a constructive superimpose radiation pattern can still hold in this condition with three EBG structures while keeping physical spacing of the array element to close to half a wavelength.

Fig. 15 shows the current diagram at the center frequency point of the simulation. As shown in this figure, the current directions at the corresponding positions of the feeding metal pillars with the same height as the four slots are all the same (red arrows). Based on the current flow in the EBG slow wave structure, it can be observed that the current is generally opposite to the current flowing at the radiation location. Additionally, the current passing through the EBG structure is approximately half a wavelength. These characteristics suggest that the reverse current does not appear significantly at the circular radiation slot, allowing the electric field of these four slots to be superimposed after radiation. The proposed filtenna generates three radiation nulls using open stubs, which is similar to the approach used in case-B filtenna. Two pairs of longer open stubs are used to generate low-frequency radiation nulls, while a short open stubs is used to create the high-frequency radiation null. The half-wavelength short-circuit effect is not utilized in this design to generate the radiation null because it is far away from the passband. By using open stubs to generate the radiation nulls, the proposed filtenna can achieve better filtering performance with a higher degree of control over the frequency response. This approach also allows for greater flexibility in adjusting the position and bandwidth of the radiation nulls, making it easier to optimize the antenna's overall performance.

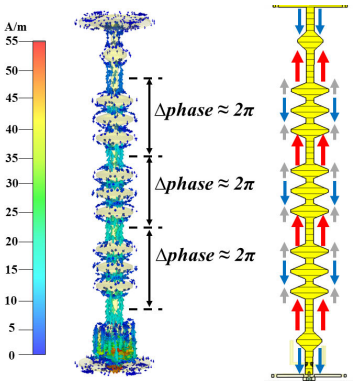

Fig. 15. In-band current diagram of the proposed antenna.

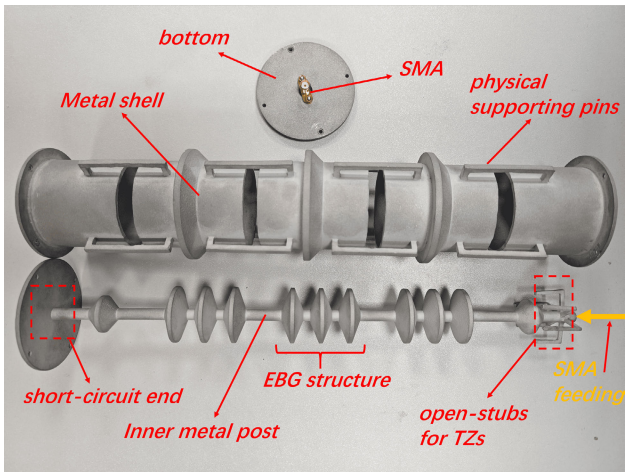

Fig. 16. Photographs of the proposed filtenna.

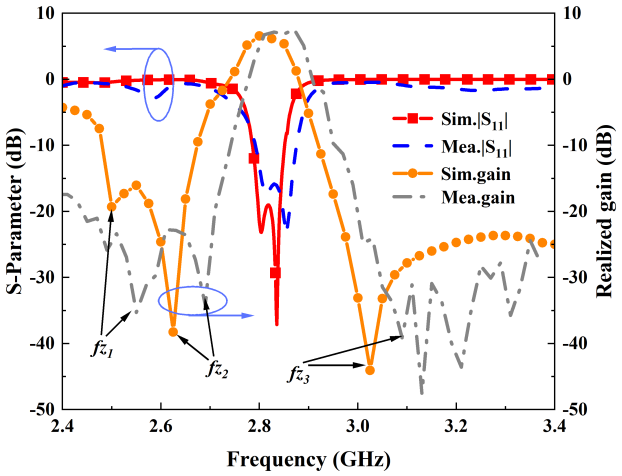

Fig. 17. Simulated and measured S parameter and gain curves of the proposed antenna.

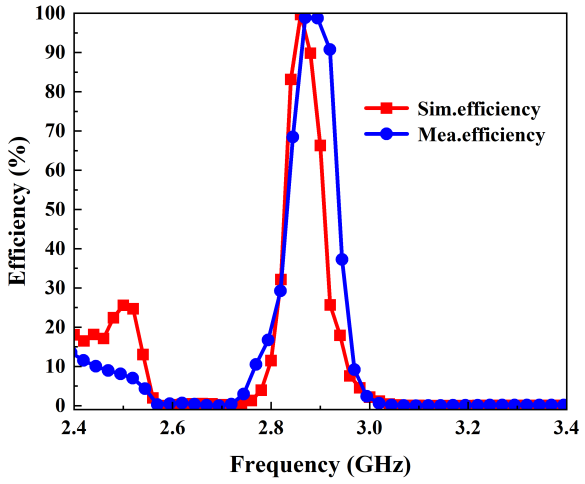

Fig. 18. Simulated and measured efficiency of the proposed filtenna.

IV. Antenna Fabrication and Measurement

In order to verify the above statement, the model of the proposed filtenna was processed and tested. Fig. 16 is the photographs of the proposed filtenna. The metal material used for 3-D printing here is aluminum alloy. Due to the complexity of the structure, it cannot be processed as a whole. Therefore, the entire antenna is divided into three parts during the full-metal 3-D printing process. The optimized dimensions of this antenna are shown in Table IV.

The measurement of S-parameters uses Keysight vector network analyzer (KEYSIGHT E5071C), and the radiation pattern and realized gain are carried out in the anechoic chamber far-field test system.

Fig. 17 presents a comparison between the simulated and measured S-parameters and gain curves of the filtenna. It should be noted that due to processing errors, the actual size of the filtenna is slightly smaller than the simulation model. This discrepancy is also reflected in the measured results shown in Fig. 17. The measured −10 dB impedance bandwidth is 3%, spanning from 2.79 to 2.875 GHz. Additionally, the peak gain in the passband is 6.6 dBi, while three nulls are observed at 2.55, 2.69, and 3.09 GHz. The measured out of band suppression has reached 28 dB, showing good filtering characteristics. The frequencies of the three nulls basically conform to the speculations of formulas (3)–(5). The results of simulation and measurement are reasonable matched to each other. Since the antenna is processed using emerging 3-D printing technology, in order to verify its reliability, Fig. 18 shows the efficiency of simulated and measured, the maximum efficiency of simulation is 98.7%, while the maximum efficiency in measured is approximately 98.1%. It can be seen that the measured efficiency is generally consistent with the simulated results except for a slight frequency shift.

Fig. 19 shows the simulated and measured E-plane and H-plane radiation patterns at the two resonant frequency points, respectively. It can be seen that the cross-polarization of the E-plane tested is not as good as simulation, the main reason is that the 3-D metal printing of the proposed filternna is not perfectly identical along the center point. As shown in Fig. 19(c) and (d), this is also reflected in the H-plane pattern, and the measured results are not as close to a perfect circle as the simulated results, which is caused by the imperfections in antenna fabrication. The pattern of the proposed antenna is similar to that of a dipole, which is explained at the beginning that the annular slot is complementary consistent with the dipole.

TABLE I
COMPARISON OF THE PROPOSED ANTENNA WITH OTHER DESIGN

Ref.	omnidirection antenna	Filtering method	FBW	gain	TZs	suppression level	manufacturing process	Antenna Size(λ_0^3)
[21]	Yes	Internal filter	1.8%	6.2 dBi	0	12.3 dBi	PCB	0.0066
[26]	No	Slots	58.3%	7.6 dBic	2	14 dBic	PCB	0.056
[27]	No	Parasitic patch + shorting post	5.1%	6.3 dBi	2	16 dBi	PCB	0.005
[28]	No	Short slot	12.6%	9.06 dBi	2	26 dBi	PCB	0.0298
[29]	No	Splitring resonator (SRR)	18.8%	9.5 dBi	2	10 dBi	PCB	0.135
[32]	No	Quarter-wavelength branch + multipath cancellation	9.71%	8.2 dBi	2	24.11 dBi	PCB	0.047
[33]	Yes	/	11.6%	11 dBi	/	/	PCB	0.046
[34]	Yes	/	20%	3 dBi	/	/	PCB	0.071
This work	**Yes**	**Open stubs**	**3%**	**6.6 dBi**	**3**	**28 dBi**	**Metal 3D Printing**	**0.2135**

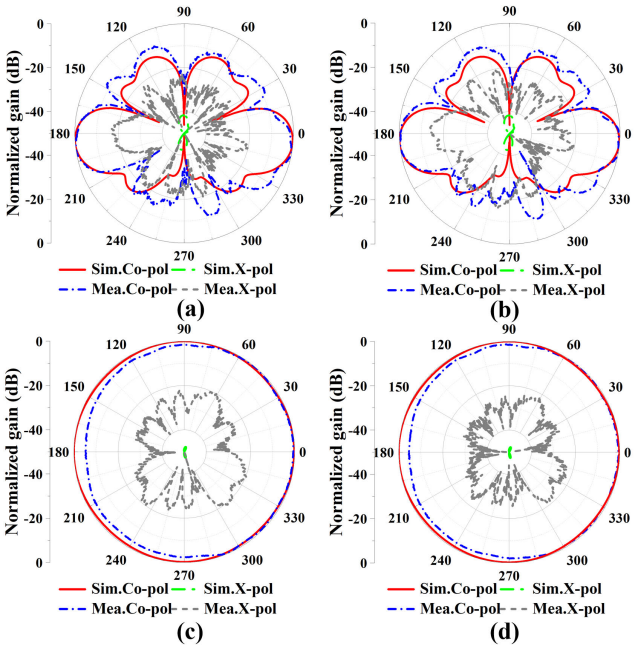

Fig. 19. Simulated and measured E-plane and H-plane pattern. (a) E-plane at the first resonant frequency point. (b) E-plane at the second resonant frequency point. (c) H-plane at the first resonant frequency point. (d) H-plane at the second resonant frequency point.

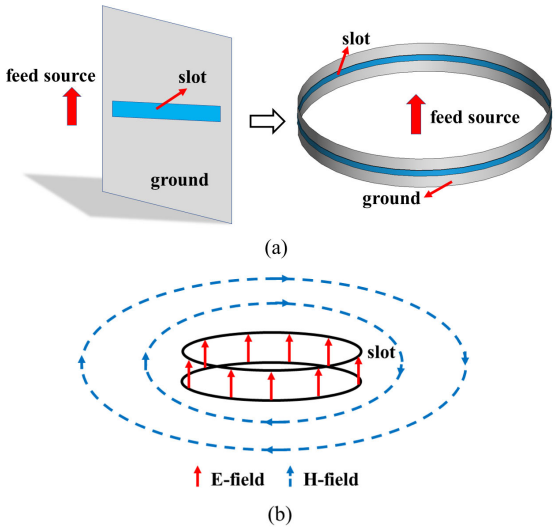

Fig. 20. Circular slot antenna. (a) Conversion diagram. (b) Electric field and magnetic field distribution.

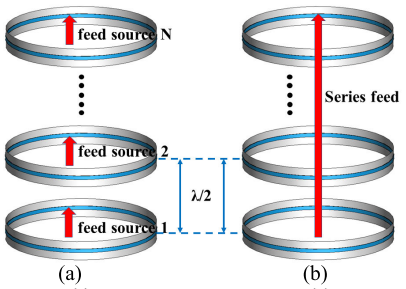

Fig. 21. Slot antenna array. (a) Independent feed. (b) Series-fed.

Table I presents a comparison between the proposed filtenna and other filtennas reported in the references. Among all the filtenna designs listed, the proposed filtenna demonstrates the highest out-of-band suppression. This superior performance can be attributed to the presence of three radiation nulls in the proposed filtenna, which surpasses the capabilities of the other filtennas listed in the table. Among those omnidirectional antennas, the bandwidth of [33] and [34] and the gain of [33] are higher than the proposed filtenna, but they do not have filtering performance. It is noteworthy that, the proposed filtenna is full-metal 3-D printing which means there is no dielectric loss and the power handling capability is higher than those PCB antennas. This is mainly due to the fact the our proposed filtenna is a full-metal high gain antenna, which has high power handling capability while the other antennas in comparison table are using planar PCB technology which of course has compact in antenna volume.

TABLE II
PARAMETERS OF THE CASE-A

Size	l_1	l_2	l_3	l_4	l_5	l_6	d_1
Value (mm)	21	6	45	6	38	5	13
Size	d_2	r	h	h_1	$wslot$		
Value (mm)	2	2.7	60	51	11		

TABLE III
PARAMETERS OF THE CASE-B

Size	l_1	l_2	l_3	l_4	l_5	l_6	d_1
Value (mm)	23.5	12	19	12	14.5	12	17.5
Size	d_2	r	rt_1	rt_2	h	h_1	h_2
Value (mm)	2	3	9.6	15	163	3.8	8.3
Size	h_3	ht_1	ht_2	hr_1	hr_2	hr_3	$wslot$
Value (mm)	6.4	14	12.8	34	60	74.5	7.6

TABLE IV
PARAMETERS OF THE PROPOSED ANTENNA

Size	l_1	l_2	l_3	l_4	l_5	l_6	d_1
Value (mm)	26.2	13.5	20.5	13.5	15.5	13.5	17.4
Size	d_2	r	hs_1	hs_3	h	h_1	h_2
Value (mm)	2	3	47	167	274	8	10.5
Size	h_3	ht_1	ht_2	hr_1	hr_2	$wslot$	
Value (mm)	6.8	14	12.8	25.2	62	7	

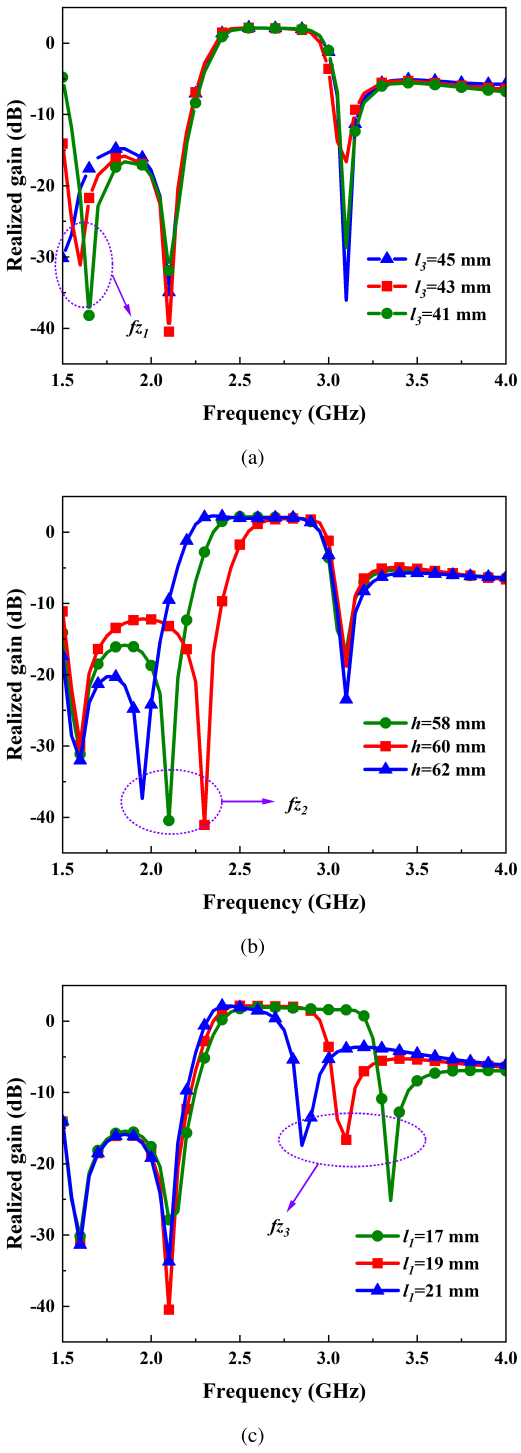

Fig. 22. Key parameter analysis of case A. (a) fz_1. (b) fz_2. (c) fz_3.

V. CONCLUSION

This article introduces a full-metal omnidirectional filtering series-fed antenna that is manufactured using 3-D metal printing technology. The antenna design is equivalent to a second-order filter circuit and incorporates three pairs of open stubs. These open stubs are strategically placed to generate three radiation nulls, thereby achieving effective out-of-band signal suppression. Importantly, the addition of these radiation nulls does not result in an increase in the overall size or complexity of the antenna circuitry. The EBG-based approach is proposed to reduce the physical dimension for achieving good radiation pattern. For verifying the proposed idea, an omnidirectional filtenna using four slots for radiation has been designed. This antenna achieves a 10-dB fractional bandwidth of 3% and has a relatively high gain, good omnidirectional radiation performance, 28 dB out-of-band rejection implies good filtering performance. Finally, this article have successfully fabricated a full-metal omnidirectional filtenna using 3-D metal printing technology. The simulation and measurement results obtained align with the design theory, confirming the effectiveness of the proposed design. The presented omnidirectional filtering antenna offers an excellent solution for achieving omnidirectional coverage in communication systems. Particularly in scenarios where the target location is unknown or constantly changing, the use of omni-

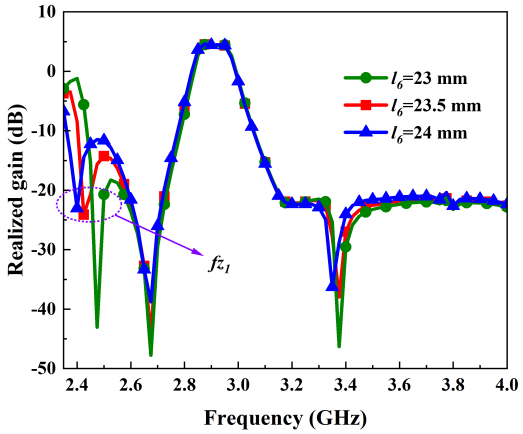

(a)

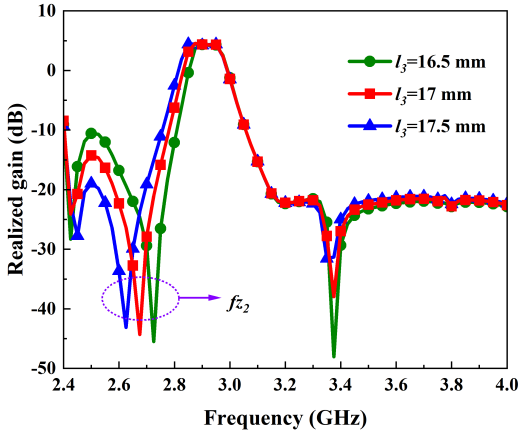

(b)

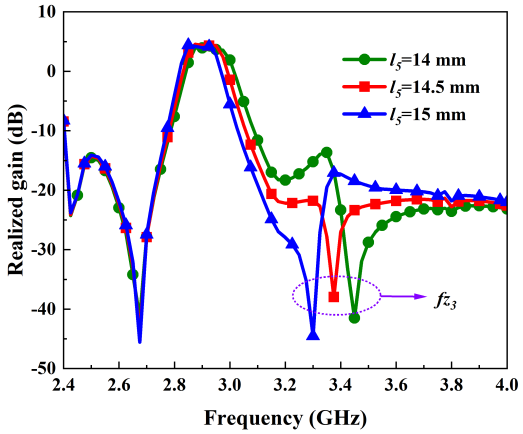

(c)

Fig. 23. Key parameter analysis of case B. (a) fz_1. (b) fz_2. (c) fz_3.

directional antennas becomes crucial. This article presents a new design solution for such antennas.

APPENDIX

To improve the overall conciseness of the article, some figures and tables will be placed in the appendix. The figures and tables are as follows.

As shown in Fig. 20(a), in order to construct an omnidirectional radiation antenna, the slot antenna can be bent into a circular ring, and the feeding source is placed at the center of the circle. According to the complementary theory, there exists a close relationship between a slot antenna and a short electric dipole. In this theory, the slot antenna can be approximated as a dipole by forming a complementary structure with it. Fig. 20(b) illustrates the EM field of an omnidirectional slot antenna, where the electric field is distributed along the vertical direction and the magnetic field is distributed along the horizontal direction. If multiple circular slot antennas are stacked vertically, an antenna array can be formed, as depicted in Fig. 21(a). In order to have good radiation pattern, two condition should be simultaneously satisfied: the same feeding source must be located at the center of the circle with equal phase, and the distance between the array radiation elements must be about half a wavelength. However, in practical application, it is difficult to use traditional power divider to feed vertical circular slot antenna practically. Thus, the series feed is used in this article to solve this problem as shown in Fig. 21(b).

Fig. 22 illustrates the analysis of some key parameters that influence the radiation nulls in the case-A. As depicted in Fig. 22(a), when the length of the long open stub l_3 is increased, the low-frequency radiation null f_{z1} shifts toward lower frequencies. Similarly, as shown in Fig. 22(b), when the height of the antenna is increased, the frequency of the radiation null f_{z2} also shifts toward lower frequencies. Likewise, when the short open-circuit stub length l_1 decreases as shown in Fig. 22(c), the high-frequency radiation null f_{z3} moves to high frequency.

Fig. 23 shows the analysis of some key parameters of case-B. As shown in Fig. 23(a), when the long open-circuit stub length l_6 gradually increases, the low-frequency radiation null f_{z1} moves to low-frequency, and when the open-circuit stub length l_3 gradually increases as shown in Fig. 23(b), fz_2 moves to low-frequency. Similarly, when the short open-circuit stub length l_5 decreases, the high-frequency radiation null f_{z3} moves to high frequency as shown in Fig. 23(c).

REFERENCES

[1] S. W. Wong, T. G. Huang, C. X. Mao, Z. N. Chen, and Q. X. Chu, "Planar filtering ultra-wideband (UWB) antenna with shorting pins," *IEEE Trans. Antennas Propag.*, vol. 61, no. 2, pp. 948–953, Feb. 2013.

[2] D. Li and C. Deng, "A single-layer filtering antenna with two controllable radiation nulls based on the multimodes of patch and SIW resonators," *IEEE Antennas Wireless Propag. Lett.*, vol. 22, no. 3, pp. 551–555, Mar. 2023.

[3] Q. Liu and L. Zhu, "A compact wideband filtering antenna on slots-loaded square patch radiator under triple resonant modes," *IEEE Trans. Antennas Propag.*, vol. 70, no. 10, pp. 9882–9887, Oct. 2022.

[4] M. Yang, B. Wu, C. Fan, H.-Y. Xie, J.-Z. Chen, and L. Wu, "Synthesis and design of filtering antenna with flexible passband and radiation null based on parallel scheme," *IEEE Antennas Wireless Propag. Lett.*, vol. 20, no. 5, pp. 838–842, May 2021.

[5] Z.-Y. Zhang et al., "Circuit model for *N*th-order filtering wire antenna, parameter extraction, and radiation prediction," *IEEE Trans. Microw. Theory Techn.*, vol. 71, no. 9, pp. 3945–3957, Sep. 2023.

[6] X. Liu, K. W. Leung, and N. Yang, "Frequency reconfigurable filtering dielectric resonator antenna with harmonics suppression," *IEEE Trans. Antennas Propag.*, vol. 69, no. 6, pp. 3224–3233, Jun. 2021.

[7] P. F. Hu, Y. M. Pan, X. Y. Zhang, and B. J. Hu, "A compact quasi-isotropic dielectric resonator antenna with filtering response," *IEEE Trans. Antennas Propag.*, vol. 67, no. 2, pp. 1294–1299, Feb. 2019.

[8] H. Tian et al., "Differentially fed duplex filtering dielectric resonator antenna with high isolation and CM suppression," *IEEE Trans. Circuits Syst. II, Exp. Briefs*, vol. 69, no. 3, pp. 979–983, Mar. 2022.

[9] N.-W. Liu, Y.-D. Liang, L. Zhu, Z.-X. Liu, and G. Fu, "A low-profile, wideband, filtering-response, omnidirectional dielectric resonator antenna without enlarged size and extra feeding circuit," *IEEE Antennas Wireless Propag. Lett.*, vol. 20, no. 7, pp. 1120–1124, Jul. 2021.

[10] P. F. Hu, Y. M. Pan, K. W. Leung, and X. Y. Zhang, "Wide-/dual-band omnidirectional filtering dielectric resonator antennas," *IEEE Trans. Antennas Propag.*, vol. 66, no. 5, pp. 2622–2627, May 2018.

[11] H.-C. Li, D.-S. La, and C. Zhang, "Wide-/dual-band omnidirectional dielectric resonator antenna with filtering function," in *Proc. IEEE 4th Int. Conf. Electron. Inf. Commun. Technol. (ICEICT)*, Aug. 2021, pp. 369–372.

[12] H. Tang, C. W. Tong, and J. X. Chen, "Differential dual-polarized filtering dielectric resonator antenna," *IEEE Trans. Antennas Propag.*, vol. 66, no. 8, pp. 4298–4302, Aug. 2018.

[13] Y. M. Pan, P. F. Hu, K. W. Leung, and X. Y. Zhang, "Compact single-/dual-polarized filtering dielectric resonator antennas," *IEEE Trans. Antennas Propag.*, vol. 66, no. 9, pp. 4474–4484, Sep. 2018.

[14] X. Sun, J. Ma, Y. Feng, J. Shi, and Z. Xu, "Compact substrate integrated waveguide filtering antennas: A review," *IEEE Access*, vol. 10, pp. 91906–91922, 2022.

[15] D. Zhao, F. Lin, H. Sun, and X. Y. Zhang, "A miniaturized dual-band SIW filtering antenna with improved out-of-band suppression," *IEEE Trans. Antennas Propag.*, vol. 70, no. 1, pp. 126–134, Jan. 2022.

[16] Q. Liu and L. Zhu, "A low-profile dual-band filtering hybrid antenna with broadside radiation based on patch and SIW resonators," *IEEE Open J. Antennas Propag.*, vol. 2, pp. 1132–1142, 2021.

[17] K. Xiang, F. Chen, and Q. Chu, "A tunable filtering antenna based on coaxial cavity resonators," *IEEE Trans. Antennas Propag.*, vol. 70, no. 5, pp. 3259–3268, May 2022.

[18] K.-R. Xiang, F.-C. Chen, and Q.-X. Chu, "Novel cavity-backed filtering antennas based on radiant metal block structure," *IEEE Trans. Antennas Propag.*, vol. 70, no. 9, pp. 7944–7953, Sep. 2022.

[19] K.-R. Xiang, F.-C. Chen, Q.-X. Chu, and Q. Xue, "High selectivity waveguide filtering antennas using mixed-mode cavity resonator," *IEEE Trans. Microw. Theory Techn.*, vol. 70, no. 9, pp. 4297–4307, Sep. 2022.

[20] C. Chen, "A compact wideband filtering omnidirectional dipole antenna without extra circuits," *IEEE Trans. Antennas Propag.*, vol. 70, no. 3, pp. 1729–1739, Mar. 2022.

[21] H. Su, L. L. Wu, Y. Zhang, J. Zhang, H. L. Xu, and X. Y. Zhang, "Circuit modeling and parameter extracting of a filtering series-fed antenna," *IEEE Trans. Microw. Theory Techn.*, vol. 71, no. 4, pp. 1640–1653, Apr. 2023.

[22] A. Abbaspour-Tamijani, J. Rizk, and G. Rebeiz, "Integration of filters and microstrip antennas," in *Proc. IEEE Antennas Propag. Soc. Int. Symp.*, vol. 2, Jun. 2002, pp. 874–877.

[23] C.-T. Chuang and S.-J. Chung, "New printed filtering antenna with selectivity enhancement," in *Proc. Eur. Microw. Conf. (EuMC)*, Sep. 2009, pp. 747–750.

[24] J.-Y. Lin, Y. Yang, S.-W. Wong, and Y. Li, "High-order modes analysis and its applications to dual-band dual-polarized filtering cavity slot arrays," *IEEE Trans. Microw. Theory Techn.*, vol. 69, no. 6, pp. 3084–3092, Jun. 2021.

[25] P. F. Hu, Y. M. Pan, X. Y. Zhang, and S. Y. Zheng, "A compact filtering dielectric resonator antenna with wide bandwidth and high gain," *IEEE Trans. Antennas Propag.*, vol. 64, no. 8, pp. 3645–3651, Aug. 2016.

[26] J. Wang, Y. Zhang, L. Ye, and Q. H. Liu, "A wideband circularly polarized filtering antenna based on slot-patch structure," *IEEE Antennas Wireless Propag. Lett.*, vol. 22, no. 8, pp. 1858–1862, Aug. 2023.

[27] K. Hu, M. Tang, D. Li, Y. Wang, and M. Li, "Design of compact, single-layered substrate integrated waveguide filtenna with parasitic patch," *IEEE Trans. Antennas Propag.*, vol. 68, no. 2, pp. 1134–1139, Feb. 2020.

[28] C. Fan, B. Wu, Y.-L. Wang, H.-Y. Xie, and T. Su, "High-gain SIW filtering antenna with low H-plane cross polarization and controllable radiation nulls," *IEEE Trans. Antennas Propag.*, vol. 69, no. 4, pp. 2336–2340, Apr. 2021.

[29] H. Yuan, F.-C. Chen, and Q.-X. Chu, "A wideband and high gain dual-polarized filtering antenna based on multiple patches," *IEEE Trans. Antennas Propag.*, vol. 70, no. 10, pp. 9843–9848, Oct. 2022.

[30] Z.-C. Guo, L. Zhu, and S.-W. Wong, "Synthesis of transversal bandpass filters on stacked rectangular H-plane waveguide cavities," *IEEE Trans. Microw. Theory Techn.*, vol. 67, no. 9, pp. 3651–3660, Sep. 2019.

[31] M. Yang, B. Wu, and L. Wu, "High selective parallel-scheme filtering antenna synthesized by transversal coupling matrix," *Int. J. RF Microw. Comput.-Aided Eng.*, vol. 32, no. 4, Jan. 2022, Art. no. 23054.

[32] S. Liu, Z. Wang, and Y. Dong, "A compact filtering patch antenna with high suppression level and its CP application," *IEEE Antennas Wireless Propag. Lett.*, vol. 22, no. 4, pp. 769–773, Apr. 2023.

[33] Z. Liang, L. Huang, W. Xu, Y. Peng, J. Wang, and H. Zhang, "Compact high gain omnidirectional horizontally polarized antenna array utilizing an aperture with uniform field distribution," *IEEE Trans. Antennas Propag.*, vol. 70, no. 11, pp. 11138–11142, Nov. 2022.

[34] Z. Zhang, S. Liao, Y. Yang, W. Che, and Q. Xue, "Low-profile and shared aperture dual-polarized omnidirectional antenna by reusing structure of annular quasi-dipole array," *IEEE Trans. Antennas Propag.*, vol. 70, no. 9, pp. 8590–8595, Sep. 2022.

[35] R.-S. Chen et al., "Reconfigurable full-metal circularly-polarized cavity-backed slot antenna and array with frequency and polarization agility," *IEEE Trans. Circuits Syst. II, Exp. Briefs*, vol. 70, no. 2, pp. 531–535, Feb. 2023.

[36] R. S. Chen et al., "Novel reconfigurable full-metal cavity-backed slot antennas using movable metal posts," *IEEE Trans. Antennas Propag.*, vol. 69, no. 10, pp. 6154–6164, Oct. 2021.

[37] R.-S. Chen et al., "S-band full-metal circularly polarized cavity-backed slot antenna with wide bandwidth and wide beamwidth," *IEEE Trans. Antennas Propag.*, vol. 69, no. 9, pp. 5963–5968, Sep. 2021.

[38] S. W. Wong and L. Zhu, "Ultra-wideband bandpass filters with improved out-of-band behaviour via embedded electromagnetic-bandgap multimode resonators," *IET Microw., Antennas Propag.*, vol. 2, no. 8, pp. 854–862, Dec. 2008.

[39] S. W. Wong and L. Zhu, "EBG-embedded multiple-mode resonator for UWB bandpass filter with improved upper-stopband performance," *IEEE Microw. Wireless Compon. Lett.*, vol. 17, no. 6, pp. 421–423, Jun. 2007.

[40] L. Zhu and K. Wu, "Short-open calibration technique for field theory-based parameter extraction of lumped elements of planar integrated circuits," *IEEE Trans. Microw. Theory Techn.*, vol. 50, no. 8, pp. 1861–1869, Aug. 2002.

Shu-Qing Zhang (Student Member, IEEE) was born in Jiangxi, China. He is currently pursuing the master's degree with the College of Electronics and Information Engineering, Shenzhen University, Shenzhen, China.

His current research interests include microwave filtering antenna and 3-D metal printing microwave circuits.

Sai-Wai Wong (Senior Member, IEEE) received the B.S. degree in electronic engineering from The Hong Kong University of Science and Technology, Hong Kong, in 2003, and the M.Sc. and Ph.D. degrees in communication engineering from Nanyang Technological University, Singapore, in 2006 and 2009, respectively.

From July 2003 to July 2005, he was an Electronic Engineer to lead the Electronic Engineering Department in China with two Hong Kong manufacturing companies. From May 2009 to October 2010, he was a Research Fellow with the ASTAR Institute for Infocomm Research, Singapore. Since 2010, he has been an Associate Professor and later become a Full Professor with the School of Electronic and Information Engineering, South China University of Technology, Guangzhou, China. Since 2017, he has been a tenured Full Professor with the College of Electronics and Information Engineering, Shenzhen University, Shenzhen, China. He has authored and coauthored more than 300 articles in international journals and conference proceedings. He is the main inventor with more than 70 authorized Chinese Invention Patents. His current research interests include RF/microwave circuit and antenna design, and integrated sensing and communication (ISAC).

Dr. Wong was a recipient of the New Century Excellent Talents in University awarded by the Ministry of Education of China in 2013 and Shenzhen Overseas High-Caliber Personnel Level C in 2018.

Zhonghe Zhang (Graduate Student Member, IEEE) was born in Jinzhong, Shanxi, China, in 1995. He received the B.S. and M.E. degrees from the North University of China, Taiyuan, China, in 2018 and 2021, respectively. He is currently pursuing the Ph.D. degree with the College of Electronics and Information Engineering, Shenzhen University, Shenzhen, China.

His current research interests include millimeter wave antennas and arrays, reconfigurable antennas and arrays, and multibeam antennas and arrays.

Yejun He (Senior Member, IEEE) received the Ph.D. degree in information and communication engineering from Huazhong University of Science and Technology (HUST), Wuhan, China, in 2005.

From 2005 to 2006, he was a Research Associate with the Department of Electronic and Information Engineering, The Hong Kong Polytechnic University, Hong Kong. From 2006 to 2007, he was a Research Associate with the Department of Electronic Engineering, Faculty of Engineering, The Chinese University of Hong Kong, Hong Kong. In 2012, he was a Visiting Professor with the Department of Electrical and Computer Engineering, University of Waterloo, Waterloo, ON, Canada. From 2013 to 2015, he was an Advanced Visiting Scholar (Visiting Professor) with the School of Electrical and Computer Engineering, Georgia Institute of Technology, Atlanta, GA, USA. From 2023 to 2024, he is an Advanced Research Scholar (Visiting Professor) with the Department of Electrical and Computer Engineering, National University of Singapore, Singapore. He was selected as a Pengcheng Scholar Distinguished Professor, Shenzhen, and a Minjiang Scholar Chair Professor of Fujian Province, in 2020 and 2022, respectively. Since 2006, he has been a Faculty Member with Shenzhen University, Shenzhen, China, where he is currently a Full Professor with the College of Electronics and Information Engineering, the Director of Guangdong Engineering Research Center of Base Station Antennas and Propagation and Shenzhen Key Laboratory of Antennas and Propagation, Shenzhen, and the Chair of IEEE Antennas and Propagation Society-Shenzhen Chapter. He has authored or coauthored over 280 research articles, seven books, and holds about 20 patents. His research interests include wireless communications, and antennas and radio frequency.

Dr. He has been a fellow of IET since 2016, a Senior Member of China Institute of Communications, since 2007, and a Senior Member of China Institute of Electronics, since 2011. He was a recipient of Shenzhen Overseas High-Caliber Personnel Level B ("Peacock Plan Award" B) and Shenzhen High-Level Professional Talent (Local Leading Talent). He received Shenzhen Science and Technology Progress Award in 2017 and Guangdong Provincial Science and Technology Progress Award for two times in 2018 and 2023 and obtained the IEEE APS Outstanding Chapter Award in 2022. He has served as a Technical Program Committee Member or the Session Chair for various conferences, including the IEEE Global Telecommunications Conference (GLOBECOM), the IEEE International Conference on Communications (ICC), the IEEE Wireless Communication Networking Conference (WCNC), and the IEEE Vehicular Technology Conference (VTC). He served as the TPC Chair of IEEE ComComAp 2021, the General Chair of IEEE ComComAp 2019. He is the Principal Investigator for over 40 current or finished research projects, including the National Natural Science Foundation of China, the Science and Technology Program of Guangdong Province and the Science and Technology Program of Shenzhen City. He is currently serving as an Associate Editor of IEEE TRANSACTIONS ON MOBILE COMPUTING, IEEE TRANSACTIONS ON ANTENNAS AND PROPAGATION, IEEE ANTENNAS AND WIRELESS PROPAGATION LETTERS, *IEEE Antennas and Propagation Magazine*, *International Journal of Communication Systems*, *China Communications*, and ZTE Communications. He has served as a reviewer for various journals, such as IEEE TRANSACTIONS ON VEHICULAR TECHNOLOGY, IEEE TRANSACTIONS ON COMMUNICATIONS, IEEE TRANSACTIONS ON INDUSTRIAL ELECTRONICS, IEEE TRANSACTIONS ON ANTENNAS AND PROPAGATION, the IEEE WIRELESS COMMUNICATIONS, the IEEE COMMUNICATIONS LETTERS, and the *International Journal of Communication Systems*.